POLITECNICO
MILANO 1863

DIPARTIMENTO DI MECCANICA

mecc

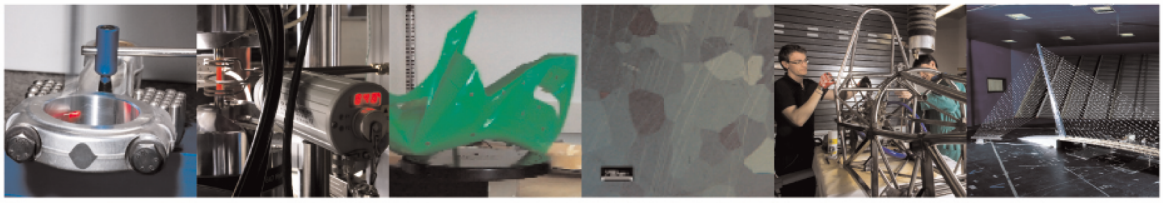

Estimating deposition efficiency and chemical composition variation along thickness for cold spraying of composite feedstocks

Ardeshiri Lordejani A.;Vitali L.;Guagliano M.;Bagherifard S.

This is a post-peer-review, pre-copyedit version of an article published in Surface and Coatings Technology. The final authenticated version is available online at: https://doi.org/10.1016/j.surfcoat.2022.128239

Estimating deposition efficiency and chemical composition variation along thickness for cold spraying of composite feedstocks

Amir Ardeshiri Lordejani, Luca Vitali, Mario Guagliano, Sara Bagherifard
Department of Mechanical Engineering, Politecnico di Milano, Milano, Italy

The low working temperature of cold spray technology offers a unique possibility to deposit a wide variety of composite materials by mixing two or more constituent powders. However, while it is possible to precisely control the chemical composition of the mixture before spraying, the compositional yield in the deposit remains uncertain. This is mainly due the variation of deposition kinetics between the constituent phases leading to a compositional deviation with respect to the feedstock. The mismatch in thermo-mechanical properties of the materials included in the feedstock, can also lead to the variation of deposit composition along its thickness. Here, we paired a probabilistic approach with finite element simulations to estimate the deposition efficiency of the mixed powder and assess the actual composition of the cold spray multi-material deposit. The developed model accounts for the interaction of the powders with the substrate and estimates the deposition probability based on the actual deformation of particles of each individual phase during deposition. The model is validated by comparison with experimental data in the case of zinc-aluminum mixture, that is known as a promising option for corrosion-resistant coatings thanks to the excellent cathodic protection. The results confirm the adeptness of the proposed model in predicting the deposition efficiency as well as deposit composition variation along the thickness with a high accuracy in the case of multi-material deposits.
Keywords: multi-material feedstock, supersonic spray, deposition efficiency, finite element modelling

Nomenclature

A_{A-A}	Splat area of an average size particle of material A upon impact onto material A
A_{A-B}	Splat area of an average size particle of material A upon impact onto material B
A_{B-A}	Splat area of an average size particle of material B upon impact onto material A
A_{B-B}	Splat area of an average size particle of material B upon impact onto material B
A_{A-s}	Splat area of an average size particle of material A upon impact onto substrate
A_{B-s}	Splat area of an average size particle of material B upon impact onto substrate
c_A	Concentration of material A based on number of particles
c_B	Concentration of material B based on number of particles
Cermet	Ceramic-Metallic (material)
CS	Cold Spray
DE	Overall deposition efficiency of the sprayed blend
DE_A	Deposition efficiency material A
DE_B	Deposition efficiency material B
f_A	Material A weight fraction in the sprayed blend
f_B	Material B weight fraction in the sprayed blend
h_A	Material A deposited layer height
h_B	Material B deposited layer height
ILA	Ideal Layer Area
KSS	Kinetic Spray Solutions (software)
LA	Layer Area
NDEP	Novel Deposition Efficiency Predictive (model)
p_{A-A}	Adhesion probability of particle A onto material A
p_{A-B}	Adhesion probability of particle A onto material B
p_{B-A}	Adhesion probability of particle B onto material A
p_{B-B}	Adhesion probability of particle B onto material B
p_{A-s}	Adhesion probability of particle A onto substrate
p_{B-s}	Adhesion probability of particle B onto substrate
RLA_A	Remaining layer area of material A
RLA_B	Remaining layer area of material B
ρ_A	Material A bulk density

ρ_B	Material B bulk density
SA_{A-A}	Relative splat area of material A sprayed onto material A
SA_{A-B}	Relative splat area of material A sprayed onto material B
SA_{B-A}	Relative splat area of material B sprayed onto material A
SA_{B-B}	Relative splat area of material B sprayed onto material B
SA_{A-s}	Relative splat area of material A sprayed onto substrate
SA_{B-s}	Relative splat area of material B sprayed onto substrate
sa_A	Relative area material A
sa_B	Relative area material B
SEM	Scanning Electron Microscope
SoD	Stand-off Distance

Introduction

As a solid-state deposition technology, cold spray offers the unique advantage of depositing composite materials by mixing two or more different constituents in the feedstock material [1], [2]. Different powders are either mechanically blended in a mixer prior to deposition or are mixed inside the spray nozzle by injection through different feeders. In the case of mixed powder deposition, numerous cases have reported deviation of the chemical composition in the deposit with respect to the feedstock mixture before spraying [3]–[6]. Since the deposition condition can be favourable for bonding of one phase while unsuitable for the other, resulting in unexpected compositional yield.

Considering the significance of deposit composition in defining its functions and performance, several models have been developed to predict the actual composition and relate it to the quantity and properties of the different materials present in the feedstock mixture. Deposition efficiency (DE) is an experimental measure defined as the ratio of weight of the deposited particles to the weight of the total sprayed feedstock. Rule of mixtures has been used to predict the DE of blended feedstock in cold spray deposits [3]. Assuming a mixture composed of two different powders, this method was used to calculate the DE of the mixture as the average of the DEs of the two powder constituents weighted by their corresponding weight fraction in the mixture. This method neglects the interaction between the dissimilar powders and assumes that the DE of individual component remains constant, regardless of its fraction in the blend. However, it has been proved that these interactions can dynamically change the DE of the blend based on the relative properties of its constituents and their weight fraction leading to a nonlinear trend in DE as the mass fraction of the powders is varied [3], [7]. The effect of powder interaction is even more evident in the case of soft-hard powder mixture, where the deposition of the sole hard material can lead to an almost zero DE, while its combination with the soft material leads to a composite deposit with the hard particles embedded into the soft matrix [8], [9].

Wu et al. [10] introduced the index of bond ratio that serves as an indicator to assess the percentage of sprayed particles that successfully adhere to a substrate upon impact. It is experimentally determined from microscopic observation of a polished surface sprayed by a single material feedstock at low feed rates and high traverse speeds (also known as splat or wipe test). The bound ratio is then calculated as the ratio of the number of the deposited particles to the total sprayed ones (deposits and craters caused by rebounded particles) or as the area of bonded splats over the area of craters and splats [9], [11]. Contrary to DE that is based on weight fraction, bond ratio is a count-type measurement. Hence a relation accounting for the particle mass and size was suggested to relate the two indexes to obtain the DE of the mixed feedstock starting from bound ratio. This method is able to implicitly account for the mutual interaction of the particles and the substrate by performing multiple splat tests and provides a good approximation of the DE [3]. This method can be used to predict the DE of virtually any mixture composition without needing to analyze the materials and mechanisms involved. However, it implies extensive experimental tests to obtain the bond ratio of the blend on substrates made of a wide range of mixed compositions. These substrates need to be all realized through cold spray deposition and then polished to obtain a smooth surface in order to provide information about the DE for feedstock mixtures of different weight fractions. Besides, the results from the splat tests are only valid for the determined composition of the feedstock materials, substrate, and cold spray process parameters (pressure, temperature, stand-off distance) and cannot be extended to any other case.

The other method, that in our opinion is the most competent available approach, was suggested in [5], [6]. Based on an empirical probability model, this approach was used to predict the DE of mixed powder

made of soft-hard constituents at steady state deposition condition for cold spray deposition. The DEs of hard and soft particles are significantly different during spraying, i.e., the DE of the soft particles can be considered constant regardless of the region of impact, whereas the hard particles' DE is affected by the substrate it locally impacts on (the already deposited soft/ hard material). This approach assumes both powders have spherical morphology, and the deformed powder (splat) areas are proportional to the original particle diameter with a proportionality coefficient that is considered the same for both constituents. It also neglects the effect of first layers of deposit in the proximity of the substrate and calculated the parameters with an assumption of steady state deposition [5], [6]. This method experimentally measures the four possible probabilities of bonding between flying soft/hard particles on already deposited soft/hard particles. Then it uses the initial composition and size of the particles in the feedstock to estimate the relative deposited areas of each constituent phase and considering their mass, provides an estimation of the resultant DE for each phase in the mixture. This model has been validated for a two-component mixture of pure copper (soft material) and cermet Cr2C3NiCr (hard) [5] deposited up to a high thickness of 3 mm in order to be able to neglect any interactions with the substrate. Despite the superior accuracy with respect to other available DE estimation approaches, this method has few major limitations. One is related to the impossibility of predicting the coating composition for low thicknesses where the effect of substrate is still relevant. This model does not account for powder interaction with substrate as it assumes a continuous and steady state process (far from the substrate). However, in practice, the interaction of individual constituent with the bare substrate induced a DE that may differ from their DE at steady state (when they are impacting the already deposited powder rather than the substrate). Consequently, the few first layers of the deposit have different compositions compared to the successive ones, causing a composition variation along the thickness. While the effect of first layer compositions can be negligible for wear-resistant coatings or cold spray additive manufacturing, it becomes more relevant for instance in applications for corrosion protection where the coating composition in the first layers is as important as the outer ones, affecting the extent of cathodic corrosion protection. The other limitation of the probability-based approach is associated with the assumption of equal splat areas for both constituents, neglecting the effect of powder morphology and specific material properties. The splat area is a function of the particle's original dimension, shape, material, impact velocity, and temperature as well as of the substrate properties. The area upon impact of different powders can significantly affect the prediction accuracy for the relative areas covered by each constituent and will in turn influence the DE of the particles sprayed in the successive layer.

Herein, we developed a new DE estimation approach by pairing a detailed finite element (FE) model with the concepts of probability-based method suggested in [5], [6] to address all the above-mentioned gaps. This hybrid numerical-semi-empirical probability-based approach reinforces the available probabilistic models for DE estimation with FE impact simulations to account precisely for the morphology and deformation behavior of the powders present in the mixture. In addition, it can predict the deposit composition along the entire deposit thickness by considering the process kinetics also during the initial transient phase of interaction with the substrate. The model has been then experimentally validated for the case of zinc-aluminum powder blend typically used for cathodic protection cold spray coatings.

2. Materials and method

2.1. Predictive model description

Th proposed model estimates the coating composition along its thickness considering the probabilities of bonding of different particles contained in the mixture to any surface they may locally impact, i.e., the substrate or the previously deposited layer of similar or dissimilar material. We assume that the particles of are well-mixed in the gas flow and the composition of each deposit layer can be estimated as a function of the composition of the one underneath (previous layer). The thickness of each deposited layer (h) is assumed to be homogeneous and constant regardless of the layer composition. Assuming a spherical shape for the particles, they will flatten upon impact and will reach a final oblate spheroid shape [6], [12]. Considering conservation of volume, the thickness of each deposited layer can be approximated as the height of an imaginary cylinder having the same volume (V_{avg}) of the particle and a diameter equal to the largest diameter of the splat (w).

$$h = \frac{4\,V_{avg}}{\pi\,w^2} \quad \text{Eq. 1}$$

In the case of a mixture containing two or more constituents (A, B, …, N), the thickness can be calculated as the average of the estimated heights of all constituent (h_A, h_B, ….h_N) weighted by the weight fraction of the corresponding material in the mixture, f.

$$\mathrm{h} = f_A \times h_A + f_B \times h_B + \cdots + f_N \times h_N \quad \text{Eq. 2}$$

The predictive model can be theoretically adapted for unlimited number of constituent materials; however, for sake of simplicity, the formulation is presented here considering a bi-component mixture made of generic materials A and B. Knowing the average initial particle diameters (d), their corresponding weight fractions in the blend (f), and the material densities (ρ), the number concentration of powder particles of materials A and B (c_A and c_B) can be defined as expressed in Eq.3 and 4, similar to the approach used in [5], [6].

$$c_A = \frac{f_A\,\rho_B\,V_B}{f_A\,\rho_B\,V_B + f_B\,\rho_A\,V_A} \quad \text{Eq. 3}$$

$$c_B = \frac{f_B\,\rho_A\,V_A}{f_A\,\rho_B\,V_B + f_B\,\rho_A\,V_A} = 1 - c_A \quad \text{Eq. 4}$$

To obtain the relative areas covered by materials A and B in each layer, the relative splat areas (SA) are required as input for the model. These are estimated for the impact of particles A and B on material A ($SA_{A\text{-}A}$ and $SA_{A\text{-}B}$), on material B ($SA_{A\text{-}B}$ and $SA_{B\text{-}B}$) and on the substrate ($SA_{A\text{-}s}$ and $SA_{B\text{-}s}$). These parameters are estimated using a detailed FE model that is described in the following section. Based on that, the relative splat area can be defined as in Eq. 5 and Eq. 6, where $A_{A\text{-}A}$ and $A_{B\text{-}A}$ are respectively the splat area of an average size particle of material A and B upon impact onto a substrate made of material A (taken from the FE model). The definition is analogous for $A_{A\text{-}B}$, $A_{B\text{-}B}$, $A_{A\text{-}s}$, and $A_{B\text{-}s}$.

$$SA_{A-A} = \frac{A_{A-A}}{A_{A-A} + A_{B-A}} \quad \text{Eq.5}$$

$$SA_{B-A} = \frac{A_{B-A}}{A_{A-A} + A_{B-A}} = 1 - SA_{A-A} \quad \text{Eq. 6}$$

The four adhesion probabilities between the similar and dissimilar particles [5], [6], and the two additional ones describing the adhesion of particles A and B on the substrate are defined as: $p_{A\text{-}A}$ as the adhesion probability of deposition of material A on A (DE of A on A), $p_{A\text{-}B}$ as the adhesion probability of deposition of material A on B (DE of A on B), $p_{B\text{-}A}$ as the adhesion probability of deposition of material B on A (DE of B on A), $p_{B\text{-}B}$ as the adhesion probability of deposition of material B on B (DE of B on B), $p_{A\text{-}s}$ as the adhesion probability of deposition of material A on substrate (DE of A on substrate) and finally $p_{B\text{-}s}$ as the adhesion probability of deposition of material B on substrate (DE of B on substrate). These probabilities are experimentally estimated as described in detail in section 2.2.
In the first layer, the deposition occurs on the bare substrate. For the sake of clarity, in this document, all the parameters described for a specific layer n will be indicated in the form $[\mathrm{data}]_n$.
The relative areas (s) indicating the percentage of area covered by each material can be then calculated based on the respective probabilities of adhesion to the substrate.

$$[s_A]_1 = \frac{p_{A-s}\,c_A\,SA_{A-s}}{p_{A-s}\,c_A\,SA_{A-s} + p_{B-s}\,c_B\,SA_{B-s}} \quad \text{Eq. 7}$$

$$[s_B]_1 = \frac{p_{B-s}\,c_B\,SA_{B-s}}{p_{A-s}\,c_A\,SA_{A-s} + p_{B-s}\,c_B\,SA_{B-s}} = 1 - [s_A]_1 \quad \text{Eq. 8}$$

While the deposition efficiencies of materials A, B, and the whole mixture on the substrate are:

$$[DE_A]_1 = p_{A-s} \quad \text{Eq. 9}$$

$$[DE_B]_1 = p_{B-s} \quad \text{Eq. 10}$$

$$[DE]_1 = f_A \times p_{A-s} + f_B \times p_{B-s} \quad \text{Eq. 11}$$

The composition of the successive (second) layer, however, is influenced by the one of the previous (first) layer. The composition is thus computed through several iterations considering the adhesion probabilities of the sprayed mixture. In the first iteration, it is imagined that a unitary surface (representing the substrate or the previously deposited layer) is sprayed with a quantity of mixed powder sufficient in theory to create an entirely covered layer (*ILA*). However, since the adhesion probabilities are not unitary, the covered surface (*LA*) will be smaller than the original one. The remaining surface area (*RLA*) (i.e., the area of the original layer still not entirely covered by this spray pass), is thus to be covered in the next iterations. In the second iteration, the fictitious sprayed mixture would be sufficient to cover the remaining layer area (*RLA*); however, it is in practice only sufficient to cover a portion of it. Hence, a third iteration is necessary and thus the iterations are repeated till full coverage is achieved. A schematic illustrating *LA*, *ILA*, and *RLA* is presented in Fig. 1. All the data calculated in a specific iteration will be indicated in the form $[(\text{data})_m]_n$, where *m* is the iteration number and *n* stands for the layer number.

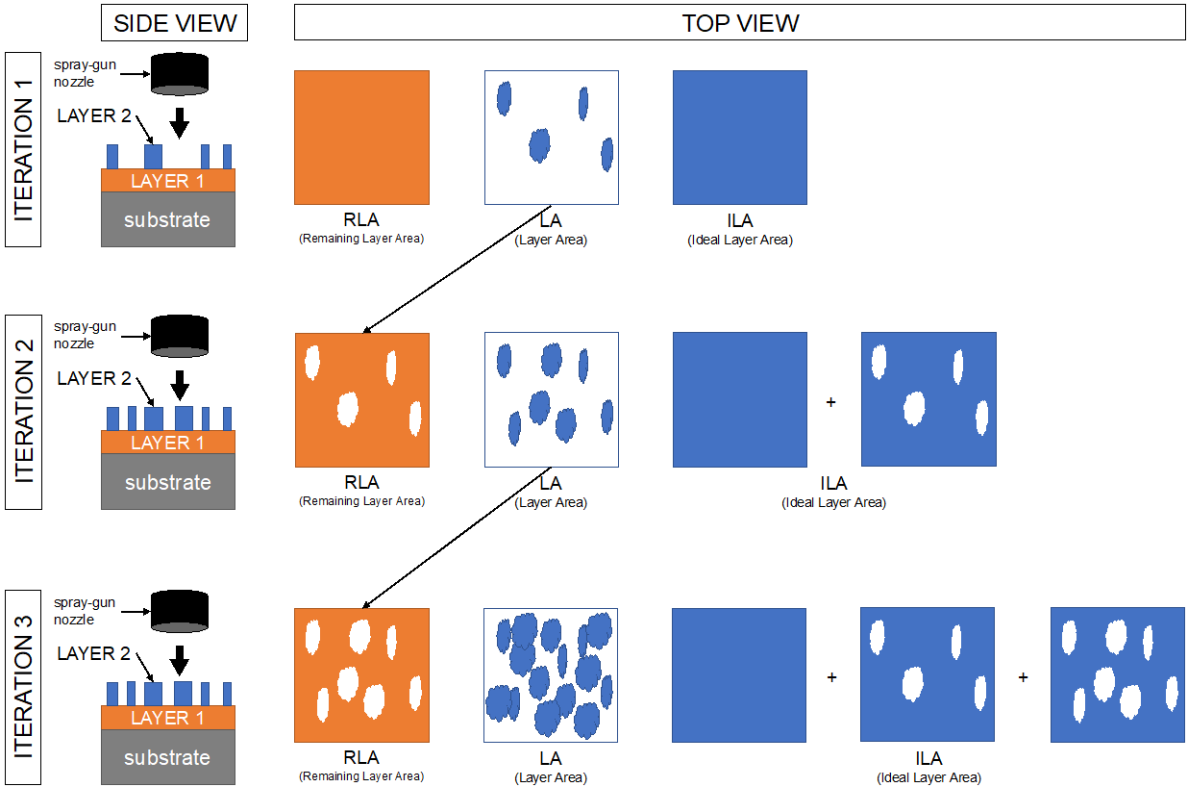

Figure 1. Schematic representation of Layer area (LA), ideal layer area (ILA), and remaining layer area (RLA) used to describe the iterative approach proposed for compositional prediction

In the second layer formation process, during the first iteration, the starting surface (indicated as the remaining layer areas of materials A and B) are equal to the relative areas of the previous layer (the first one), as expressed in Eq. 12 and Eq.13:

$$[(RLA_A)_1]_2 = [s_A]_1 \quad \text{Eq. 12}$$

$$[(RLA_B)_1]_2 = [s_B]_1 \quad \text{Eq. 13}$$

Thanks to the adhesion probabilities, the areas of the newly formed portions of the layer covered by each material in the mixture can be computed. In Eq. 14, the notation $LA_{A\text{-}on\text{-}A}$ is representing the area of the newly formed layer covered by material A on top of the area that was originally covered by material A. Similarly, in Eq. 15, $LA_{A\text{-}on\text{-}B}$ is representing the area of the new layer covered by material A on top of the area priorly covered by material B. The definition is analogous for $LA_{B\text{-}on\text{-}A}$ and $LA_{B\text{-}on\text{-}B}$.

$$[(LA_{A\ on\ A})_1]_2 = c_A\ p_{A-A}\ [(RLA_A)_1]_2\ SA_{A-A} \quad \text{Eq. 14}$$

$$[(LA_{A\ on\ B})_1]_2 = c_A\ p_{A-B}\ [(RLA_B)_1]_2\ SA_{A-B} \quad \text{Eq. 15}$$

$$[(LA_{B\ on\ A})_1]_2 = c_B\ p_{B-A}\ [(RLA_A)_1]_2\ SA_{B-A} \quad \text{Eq. 16}$$

$$[(LA_{B\ on\ B})_1]_2 = c_B\ p_{B-B}\ [(RLA_B)_1]_2\ SA_{B-B} \quad \text{Eq. 17}$$

The area that would have been ideally covered by materials A and B (*ILA*) (if all the adhesion probabilities were unitary) can be expressed as follows:

$$[(ILA_A)_1]_2 = c_A\ \{[(RLA_A)_1]_2\ SA_{A-A} + [(RLA_B)_1]_2\ SA_{A-B}\} \quad \text{Eq. 18}$$

$$[(ILA_B)_1]_2 = c_B\ \{[(RLA_A)_1]_2\ SA_{B-A} + [(RLA_B)_1]_2\ SA_{B-B}\} \quad \text{Eq. 19}$$

Intuitively after the first iteration the formation of the second layer is not completed, and the remaining layer areas, for the second iteration, can be calculated as follows:

$$[(RLA_A)_2]_2 = [s_A]_1 - \{[(LA_{A\ on\ A})_1]_2 + [(LA_{B\ on\ A})_1]_2\} \quad \text{Eq. 20}$$

$$[(RLA_B)_2]_2 = [s_B]_1 - \{[(LA_{A\ on\ B})_1]_2 + [(LA_{B\ on\ B})_1]_2\} \quad \text{Eq. 21}$$

The total layer areas covered after the second iteration can be calculated building upon the previously calculated remaining areas.

$$[(LA_{A\ on\ A})_2]_2 = c_A\ p_{A-A}\ \{[(RLA_A)_1]_2 + [(RLA_A)_2]_2\}\ SA_{A-A} \quad \text{Eq. 22}$$

$$[(LA_{A\ on\ B})_2]_2 = c_A\ p_{A-B}\ \{[(RLA_B)_1]_2 + [(RLA_B)_2]_2\}\ SA_{A-B} \quad \text{Eq. 23}$$

$$[(LA_{B\ on\ A})_2]_2 = c_B\ p_{B-A}\ \{[(RLA_A)_1]_2 + [(RLA_A)_2]_2\}\ SA_{B-A} \quad \text{Eq. 24}$$

$$[(LA_{B\ on\ B})_2]_2 = c_B\ p_{B-B}\ \{[(RLA_B)_1]_2 + [(RLA_B)_2]_2\}\ SA_{B-B} \quad \text{Eq. 25}$$

The total area that would have been ideally covered after the first and second iterations if the adhesion probabilities were unitary is:

$$[(ILA_A)_2]_2 = c_A\ \{[(RLA_A)_1]_2\ SA_{A-A} + [(RLA_B)_1]_2\ SA_{A-B} + [(RLA_A)_2]_2\ SA_{A-A} + [(RLA_B)_2]_2\ SA_{A-B}\} \quad \text{Eq. 26}$$

$$[(ILA_B)_2]_2 = c_B\ \{[(RLA_A)_1]_2\ SA_{B-A} + [(RLA_B)_1]_2\ SA_{B-B} + [(RLA_A)_2]_2\ SA_{B-A} + [(RLA_B)_2]_2\ SA_{B-B}\} \quad \text{Eq. 27}$$

The iteration process can be generalized for the mth iteration as follows:

$$[(RLA_A)_m]_2 = [s_A]_1 - \sum_{i=1}^{m-1} [(LA_{A\ on\ A})_i]_2 + [(LA_{B\ on\ A})_i]_2 \quad \text{Eq. 28}$$

$$[(RLA_B)_m]_2 = [s_B]_1 - \sum_{i=1}^{m-1} [(LA_{A\ on\ B})_i]_2 + [(LA_{B\ on\ B})_i]_2 \quad \text{Eq. 29}$$

$$[(LA_{A\ on\ A})_m]_2 = c_A\ p_{A-A} \left\{ \sum_{i=1}^{m} [(RLA_A)_i]_2 \right\} SA_{A-A} \quad \text{Eq. 30}$$

$$[(LA_{A\ on\ B})_m]_2 = c_A\ p_{A-B} \left\{ \sum_{i=1}^{m} [(RLA_B)_i]_2 \right\} SA_{A-B} \quad \text{Eq. 31}$$

$$[(LA_{B\ on\ A})_m]_2 = c_B\ p_{B-A} \left\{ \sum_{i=1}^{m} [(RLA_A)_i]_2 \right\} SA_{B-A} \quad \text{Eq. 32}$$

$$[(LA_{B\ on\ B})_m]_2 = c_B\ p_{B-B} \left\{ \sum_{i=1}^{m} [(RLA_B)_i]_2 \right\} SA_{B-B} \quad \text{Eq. 33}$$

$$[(ILA_A)_m]_2 = c_A \left\{ \sum_{i=1}^{m} [(RLA_A)_i]_2\ SA_{A-A} + [(RLA_B)_i]_2\ SA_{A-B} \right\} \quad \text{Eq. 34}$$

$$[(ILA_B)_m]_2 = c_B \left\{ \sum_{i=1}^{m} [(RLA_A)_i]_2\ \ SA_{B-A} + [(RLA_B)_i]_2\ SA_{B-B} \right\} \quad \text{Eq. 35}$$

After the mth iteration, supposing that the whole area of the 2nd layer is covered, the DEs of materials A and B as well as their relative areas in the second layer can be computed, as below:

$$[DE_A]_2 = \frac{[(LA_{A\ on\ A})_m]_2 + [(LA_{A\ on\ B})_m]_2}{[(ILA_A)_m]_2} \quad \text{Eq. 36}$$

$$[DE_B]_2 = \frac{[(LA_{B\ on\ A})_m]_2 + [(LA_{B\ on\ B})_m]_2}{[(ILA_B)_m]_2} \quad \text{Eq. 37}$$

$$[s_A]_2 = [(LA_{A\ on\ A})_m]_2 + [(LA_{A\ on\ B})_m]_2 \quad \text{Eq. 38}$$

$$[s_B]_2 = [(LA_{B\ on\ A})_m]_2 + [(LA_{B\ on\ B})_m]_2 \quad \text{Eq. 39}$$

Analogously, for the next layer, the starting area for the first iteration of the third layer is set equal to the relative areas of A and B obtained for the second layer. Hence the iteration can be started again and repeated up to the formation of the nth layer corresponding to the final desired coating thickness.
In this way, the model can predict the DEs and the relative areas of each one of the materials contained in the mixture per layer in the coating. Since the densities of the materials are known, it is thus possible to predict the weight composition in each layer. The workflow of the presented predictive model is described in Fig. 2.

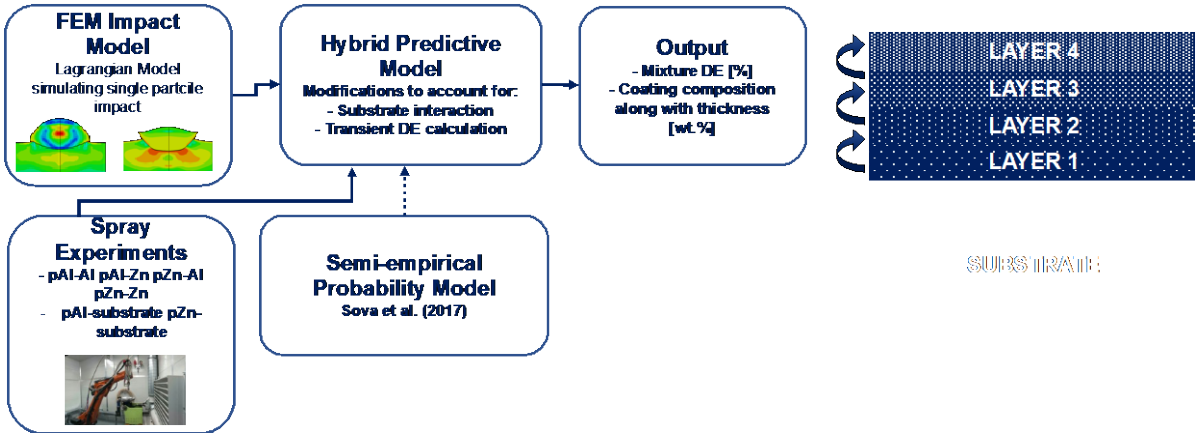

Figure 2. The developed predictive model workflow

2.2. Experimental tests

The spray tests were performed using ISS 5/8 Impact cold spray system (impact Innovations, DE). The system is equipped with a de Laval converging-diverging nozzle OUT1 (Impact Innovations, DE) of 160 mm length and expansion ratio (defined as the ratio between the outlet area and the throat) of 5.60. The substrate was a planar mild carbon steel (50x50 mm). The substrates, prior to coating, were mechanically grinded to obtain a surface roughness of Ra= 0.7 µm and subsequently cleaned with isopropyl alcohol.

Pure Zinc powder (> 99.9%) feedstock (Grillo, DE) consisted of less than 10% of particles having a diameter larger than 45 µm, 63% between 25-45 µm, and the rest smaller than 25 µm, yielding an average particle diameter of 27.2 µm and apparent density of 2.9 g/ml. Pure aluminum powder (Toyal Europe, FR) had a reported size distribution of 10% having a size smaller than 20 µm, 50% smaller than 32.6 µm, and 90% smaller than 53.4 µm, with an apparent density of 1.4 g/ml (See Fig. A1). The powders were sprayed using Nitrogen as the process gas at a stagnation pressure of 2.5 MPa and temperature of 300 °C. The stand-off distance was fixed at 25 mm for all tests.

Regarding the composition, different proportions of Al-Zn have been studied in the literature (20% Al-80% Zn, 30% Al-70% Zn, and 40% Al-60% Zn) for corrosion protection of steel substrates [13]–[15]. These studies reported a trade-off between cathodic protection and strength revealing that the mixtures with a higher percentage of Zn will provide higher cathodic protection while the ones with higher aluminum content are expected to show a better structural integrity. Based on these studies, the optimal mixture is expected to have a Zn weight percentage ranging between 30-60%, and balance Al [13]–[15].

However, there is another aspect that should be considered and that is the feasibility of obtaining a high-quality deposit as a function of the chemical composition of the blend. To identify these limits, the range of the parameters used in the available experimental data in the literature was studied and used as a starting point for our experiment (Table A1). As shown in Table A1, the stagnation temperature has been varied between 290 to 500 °C [13]–[15].

Increased gas temperature leads to more notable particle heating and thus larger deformation upon impact. Deformation is beneficial to reduce the porosity of the deposit and thus improve its corrosion resistance. However, temperature is limited by the low melting point of Zn particles (420°C), as the softened Zn particles can stick to the nozzle's internal surface causing clogging. This issue was more noted for higher Zn fraction in the blend. Higher gas pressure also is more beneficial for reduced porosity and thus higher corrosion protection; however, an excessive pressure is reported to lead to a reduced DE for Zn deposition, as the high impact velocity of the incoming particles may erode the previously deposited ones [16]. According to these analyses, in this study, feedstock blends including 0, 40, 60 and 100% Zn and balance Al were selected for DE evaluation to be later assessed for their corrosion resistance performance. Based on our initial analysis mechanical properties of the deposits, the stagnation pressure and temperature were set to 2.5 MPa and 300 °C, respectively.

The DE predictive model lays its foundations on the adhesion probabilities of the powders composing the mixture on the substrate or already deposited powders of different types. In practice, the probability is defined per each constituent as the ratio between the mass increase of the specimen and the total

sprayed powder. For deposition probability and overall DE estimation, the specimen's mass increase after deposition was measured on a calibrated scale (Gibertini EU-C7500, with accuracy equal to 0.1 g). The mass of the sprayed powder was estimated using the integrated software in the spray system based on the imposed feed rate and the spraying time or as the weight difference of the powder feeder.
The bonding probabilities were tested by spraying pure zinc and aluminum powders on different substrates to estimate the following adhesion probabilities (as schematically shown in Fig. 3):

- $p_{Al\text{-}Al}$: the adhesion probability of aluminum on aluminum
- $p_{Al\text{-}Zn}$: the adhesion probability of aluminum on zinc
- $p_{Al\text{-}substrate}$: the adhesion probability of aluminum on a substrate made of steel
- $p_{Zn\text{-}Zn}$: the adhesion probability of zinc on zinc
- $p_{Zn\text{-}Al}$: the adhesion probability of zinc on aluminum
- $p_{Zn\text{-}substrate}$: the adhesion probability of zinc on a substrate made of steel

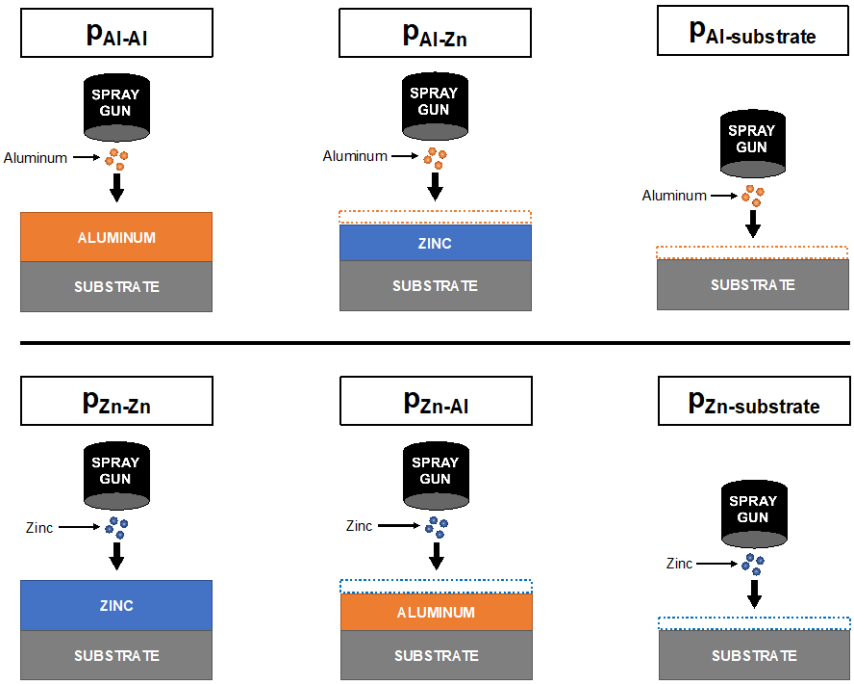

Figure 3. Schematic representation of adhesion probabilities for Al-Zn feedstock

To calculate the adhesion probability of each component of the mixture on the same material, the tests were performed by spraying on a thick deposit of the same material so that the interactions with the substrate could be null. For $p_{Al\text{-}Al}$ determination, aluminum was sprayed on a thick deposit of aluminum with a traverse speed of 30 mm/s and a hatch distance of 2 mm. When depositing a thick layer of zinc to serve as the substrate for assessing $p_{Zn\text{-}Zn}$, to avoid delamination of the zinc deposit due to the limited bonding to the substrate and high residual stresses [16] a higher traverse speed of 300 mm/s was considered increasing the number of passes. The experimental determination of the adhesion probabilities on the substrate was performed by spraying each material directly on the bare substrate. Thus, $p_{Zn\text{-}steel}$ and $p_{Al\text{-}steel}$ were determined using a traverse speed of 200 mm/s with a hatch distance of 8 mm trying to minimize the deposit thickness and avoid overlap between different passes. Hence, the majority of the impacts could be assumed to be between the flying particle and the substrate.
Considering the adhesion probability of a material on a substrate of dissimilar material, a single layer of a material was deposited on a specimen previously fully coated with the other material. The objective was to make sure that the particles of the first material impact just the second one and do not interfere with the substrate or themselves. Thus, $p_{Zn\text{-}Al}$ was measured depositing zinc on aluminum substrate at a traverse speed of 300 mm/s, to reduce the probability of particles interaction. Since zinc and aluminum are both soft materials, their impact type is assumed to be similar and therefore $p_{Al\text{-}Zn}$ was assumed equal to $p_{Zn\text{-}Al}$, as also suggested in [5].

The DE tests for mixed powders were then performed by spraying mechanically blended powder of Zn40%-Al60%, and Zn60%-Al40% on steel substrates.
For microscopy observations of cross sections, the sample were cut, englobed in a thermoset epoxy resin reinforced with glass fibers (Hitech Europe, IT), and mechanically ground with 600, 800, 1200, and 2500 grit sandpapers. The final polishing step using diamond paste was avoided to maintain the surface oxide layer that makes the darker aluminum phase distinguishable from zinc. A Leitz Wetzlar Aristomet optical microscope (OM) and a Zeiss Evo 50 scanning electron microscope (SEM) were used for microstructural observations.

2.3. Finite element model description

Single particle impact was simulated to analyze the splats' deformed shape based on their material properties and morphology. The aim was to estimate the relative splat area of particles to be used as input for the DE prediction model.
The simulations were performed using the commercial FE software ABAQUS/Explicit. Arbitrary Lagrangian-Eulerian (ALE) technique was employed due to its capability of retaining a high precision even in the presence of large material distortion, as in the case of particle impact during cold spray. The analysis considered strain hardening, strain-rate hardening, and temperature effects.
To accurately model this non-linear dynamic impact, the materials' elastic behavior was described by the Mie-Grüneisen equation of state and their plastic response under large plastic deformation and elevated strain rates was described by the Johnson-Cook plasticity model [17], [18]. The thermal behavior of the materials was described by specific heat and conductivity. Since Equation of state (EoS) was considered for all the materials, the inelastic heat fraction was set to 1 by default, assuming that all of the kinetic energy is converted into heat and then dissipated [19]. For detailed description of the material models, the reader is referred to our previous studies on numerical modelling of cold spray process [6]. The parameters required for the material models for pure aluminum were taken from [19]; the physical properties of zinc were obtained using MPDB software (JAHM Software Inc., USA), while the equation of state parameters were taken from [20]. The Johnson-Cook material model parameters for zinc were estimated from stress-strain curves at different strain rates reported in [21]. The properties of steel, as the substrate material, were taken from [22] for the simulations involving interactions with the substrate. All the material parameters are reported in Tables A2-A4.
A 2D axisymmetric model was employed for single impact analysis due to its high computational efficiency. While being aware of the geometrical deviation of the particles from spherical morphology, considering the complexity of defining a representative irregular shape, we opted for spherical shapes in the simulation for both powders. In each case, the particle was modeled as a sphere with average diameter corresponding to the employed powder in the experimental tests, i.e., 27.2 μm and 32.6 μm for Zinc and Aluminum particles, respectively. The substrate was considered as a cylinder with a radius equal to five times the radius of the particle. The impact of the particle was assumed to happen normal to the substrate surface, considering that in the experiments the nozzle was kept perpendicular to the substrate. Axisymmetric boundary conditions were imposed, and the bottom face of the substrate was fully fixed.
The particle was positioned in correspondence with the center of the substrate, with an initial distance of 1 μm between its bottom surface and substrate's upper one. The initial velocity of the particle was determined using the commercial simulation software from Kinetic Spray Solutions (KSS GmbH, Buchholz, Germany), imposing the nozzle geometry and process parameters considered in the experiments. KSS software estimates the particle impact velocity through computational fluid dynamic (CFD) simulations of the two-phase flow [23]. The initial temperature of the substrate and the particle was set at room temperature (25 °C = 298 K). The interaction consisted of a simple hard contact in the normal direction and a friction coefficient equal to 0.3 to consider possible temperature increment deriving from kinetic energy dissipated through friction [19].
Based on mesh convergence analysis, the mesh size in the particle and the central area of the substrate was set at $1/25^{th}$ of powder particle radius. The global mesh size in other regions of the substrate was 10 μm. 4-node bilinear coupled displacement-temperature quadrilateral elements, with reduced integration and hourglass control (CAX4RT) were used both for the substrate and the particle. Fig. 4, represents a view of the model with meshed particle and substrate.

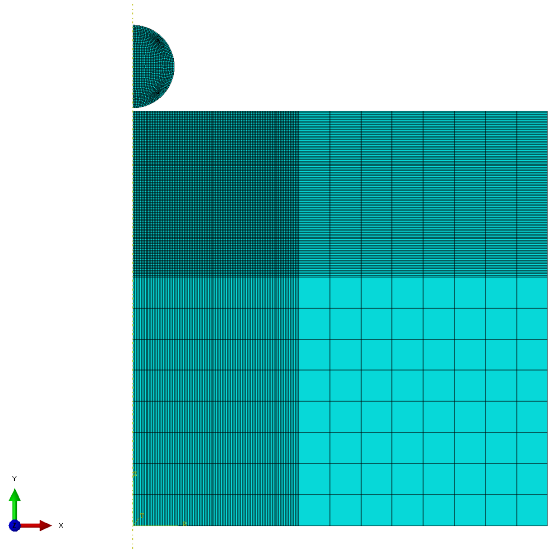

Figure 4. Single impact 2D axisymmetric model with meshed particle and substrate

In order to avoid the introduction of numerical errors in the state of plastic strain, temperature variation, or unrealistic deformation and jetting region, fine meshes, frequent remeshing and sweeps were avoided. To validate the employed FE model, its results were directly compared to the experimental results reported by Tiamiyu et. Al. [12] for single particle impact of Al on Al to validate the model. Comparisons showed a very good agreement between this experiment and our numerical results in terms of particle height and flattening ratio, proving the reliability of the FE model (see Fig. A2).

3. Results and discussion

3.1. Sample analysis

Fig. 5a and b exhibit SEM microstructural observations of the structures composed of an aluminum matrix with homogeneously dispersed zinc particles for both Zn40%-Al60% and Zn60%-Al40% deposits.

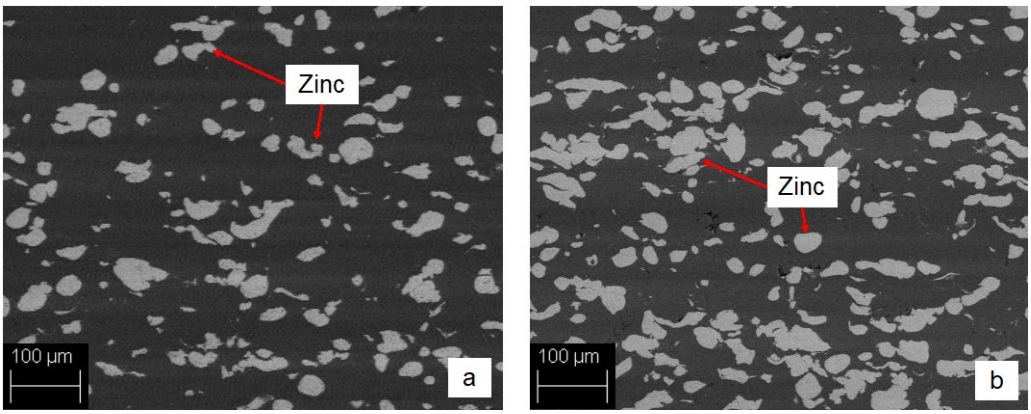

Figure 5. SEM micrographs of a) Zn40%-Al60% and b) Zn60%-Al40% deposits sprayed at 300 C and 2.5 MPa (zinc particles (bright gray) are dispersed in the aluminum matrix (dark region))

The deposit thickness was measured as an average between at least eight random measurements in different positions of the deposit. The obtained thickness was 820 µm for the Zn40%-Al60% and 770 µm for the Zn60%-Al40%. The composite materials are by definition microscopically inhomogeneous. However, considering a sufficiently large portion of material, repetition of the structural patterns can be noted in the cross sections. While spraying composite feedstock the objective is to obtain a uniform distribution of the different materials across the coating. The zinc-aluminum coating homogeneity has been quantitatively assessed by calculating each constituent's fractional area in at least 12 random cross-sectional images. Square regions of 300×300 µm were selected and

processed with ImageJ (NIH, US) to estimate the area covered by each phase, as shown by a representative image in Fig. 6.

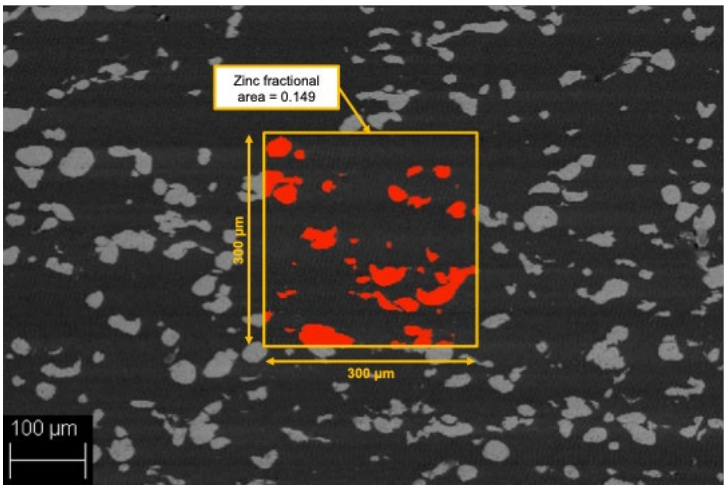

Figure 6. Example of zinc fractional area calculation over a square region of 300 x 300 µm^2 in Zn60%-Al40%. (Zinc areas are highlighted in red)

The results of image analysis presented in Table 1 indicate that the zinc particle dispersion in the aluminum matrix can be considered homogenous and practically constant in the entire coating, when exploring regions of 300 ×300 µm^2 or larger. In practice there are no regions lacking zinc particles, and thus in terms of functionality for anti-corrosion properties the coating is expected to guarantee cathodic protection in all the points. A similar conclusion can be drawn for Zn60%-Al40% where the zinc average fractional area is higher and considered to be homogeneously distributed in the coating.

Table 1. Zinc and aluminum phases distribution

Composition	Zn average fractional area	Al average fractional area	Standard deviation
Zn40%-Al60%	0.15	0.85	0.0193
Zn60%-Al40%	0.26	0.74	0.0260

Based on the procedure previously described the adhesion probabilities were experimentally determined as $p_{Zn\text{-}Zn}$ = 0.45, $p_{Al\text{-}Al}$ = 0.69, $p_{Zn\text{-steel}}$ = 0.22, $p_{Al\text{-steel}}$ = 0.57, $p_{Zn\text{-}Al}$ =0.56 and $p_{Al\text{-}Zn}$ = 0.56.

3.2. Numerical results

For overall DE calculation, the relative area covered by each constituent was determined through FE analysis. As an input for the simulations, the velocity of each particle based on its morphology and the process parameters (gas pressure and temperature) were extracted from KSS simulations. The resulting velocities for zinc and aluminum particles were respectively 493 and 523 m/s. The models were developed considering zinc and aluminum particles having diameters equal to the average of the sprayed powder. In the case of zinc-aluminum mixtures deposited on a steel substrate the six relevant splat areas are: $SA_{Zn\text{-}Al}$, $SA_{Al\text{-}Al}$, $SA_{Zn\text{-}Zn}$, $SA_{Al\text{-}Zn}$, $SA_{Zn\text{-steel}}$, and $SA_{Al\text{-steel}}$. Thus, the corresponding simulations were performed for zinc and aluminum particles impacting steel, Zinc and aluminum substrates (to simulate the impact of the particles on regions covered by previously deposited particles). Fig. 7 shows the resulting deformation upon impact for aluminum and zinc particles on steel substrate.

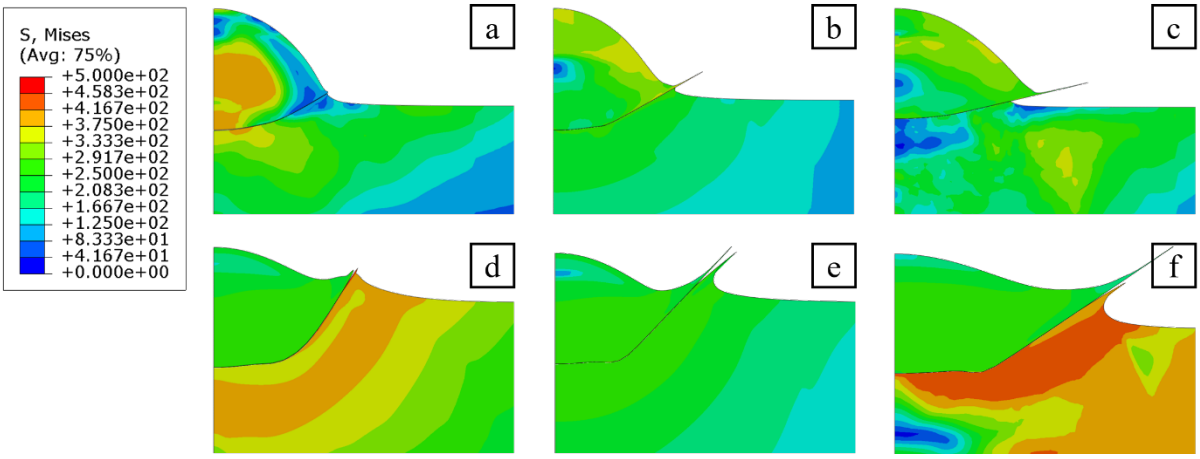

Figure 7. Deformation contour from single particle impact simulations of aluminum particle onto a) aluminum, b) zinc, and c) steel substrates, and zinc particle onto d) aluminum, e) zinc, and f) steel substrates.

The diameters of the deformed particles extracted from the impact simulations are summarized in Table 2 and were used for estimating the relative splat areas. Recalling the generic Eq. 5 and 6, e.g., in the case of zinc impacting on an aluminum substrate, the relative splat area of zinc can be defined as the ratio between the zinc splat area ($A_{Zn\text{-}Al}$) and the sum of the zinc and aluminum splat areas ($A_{Zn\text{-}Al} + A_{Al\text{-}Al}$). The relative areas for all six configurations are presented in Table 2.

Table 2. Splat areas extracted from FE simulation and estimated relative splat areas (SA) of zinc and aluminum particles upon impact considering at real particle impact velocity and aluminum, zinc, and steel as substrates

Particle material	Substrate material	Undeformed diameter [µm]	Deformed diameter [µm]	Splat area [µm^2]	Relative splat area (SA)
Zinc	Aluminum	27.20	38.68	1175.07	0.46
Aluminum	Aluminum	32.60	41.55	1355.91	0.54
Zinc	Zinc	27.20	44.72	1570.70	0.48
Aluminum	Zinc	32.60	46.86	1724.62	0.52
Zinc	Steel	27.20	47.84	1797.51	0.44
Aluminum	Steel	32.60	53.48	2246.32	0.56

3.3. Model validation

The model was validated for two compositions of Zn40-Al60% and Zn60%-Al40%. The results of the model predictions presented in Fig. 8 indicate the good approximation of the model for DE of mixed powder with a slight overestimation compared to the experimentally measured DE. This could be caused by the irregular morphology of the powder particles that was not considered in the numerical model, due to the complexity of defining a representative geometry. The predictions are well inside the confidence interval of the results. The almost linear trend could be attributed to some extent to the limited number of studied compositions. Considering additional fractions for the constituent phases will offer a more accurate prediction of the trend.

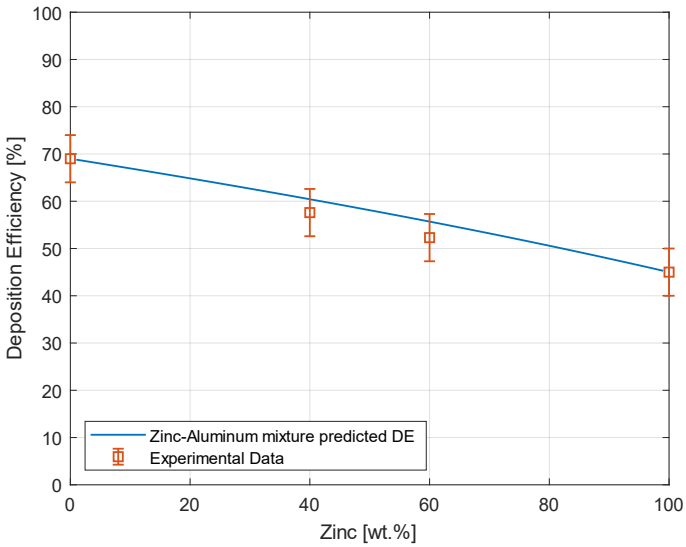

Figure 8. Comparison between the predicted DE and the experimentally measured DE for Zn40%-Al60% and Zn60%-Al40% mixtures

A special feature of the developed model is the possibility of predicting the variation of coating chemical composition along its thickness. Due to possible differences in the thermomechanical properties of the feedstock constituents, the coating composition may not be uniform through the thickness especially close to the substrate (Fig. 9). The different adhesion probabilities of zinc and aluminum on the steel substrate and on same material, led to inhomogeneous coating composition along its thickness. In particular, since the adhesion probability of zinc on steel substrate was measured to be lower than aluminum on steel, a higher concentration of aluminum is expected in the proximity of the substrate.

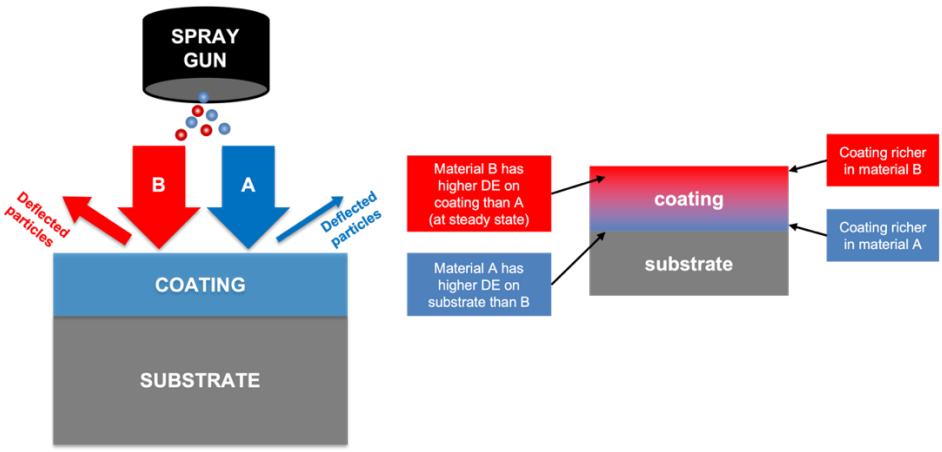

Figure 9. Schematic representation of compositional variation along thickness for mixed powder deposits

To validate the prediction of the chemical composition of the coating through its thickness, cross-section (18x10 mm^2) of specimens realized with Zn40%-Al60% powder mixture was analyzed, as presented in Fig. 10. the OM micrographs provide a qualitative confirmation of the validity of the model that predicts a low zinc content in the proximity of the substrate. The lower zinc content in the immediate proximity of the steel substrate is clear in Fig. 10. The bright 'islands' of zinc become present mostly at 40-50 µm above the steel substrate.

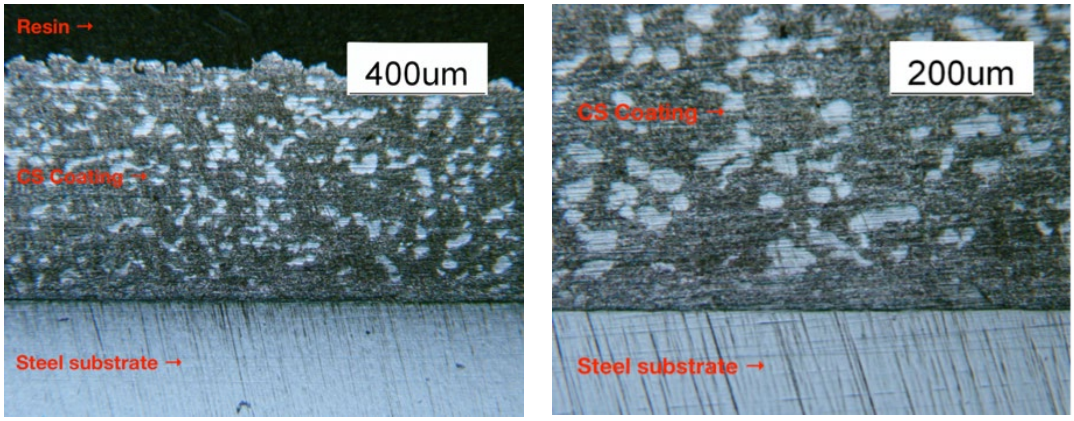

Figure 10. OM micrographs of Zn40%-Al60% specimen at different enlargements

For a quantitative confirmation, ImageJ software (NIH, US) was used to estimate the area fraction of zinc and aluminum in a thin layer in different zone of the deposit: the proximity of the steel substrate (0-30) µm, just above the substrate (30-60 µm) and after a certain thickness above which the coating composition was supposed to be stable (200-300 µm). The three regions are evidenced in the original image in Fig. 11 in red rectangles. In the image processed with Image J zinc areas (brighter spots in the original image) are highlighted in red, while the aluminum is in white. Thus, the surface area covered by zinc and aluminum were individually estimated and converted to the wt.% in the deposit considering the corresponding densities. Five random images were analyzed following the described procedure to better estimate the coating composition and account for possible variations in different areas. The coating compositions obtained in correspondence of the three zones were compared with the model's predictions, as presented in Fig. 12. The results affirm that the model can provide a reasonable estimation of the coating chemical composition along its thickness.

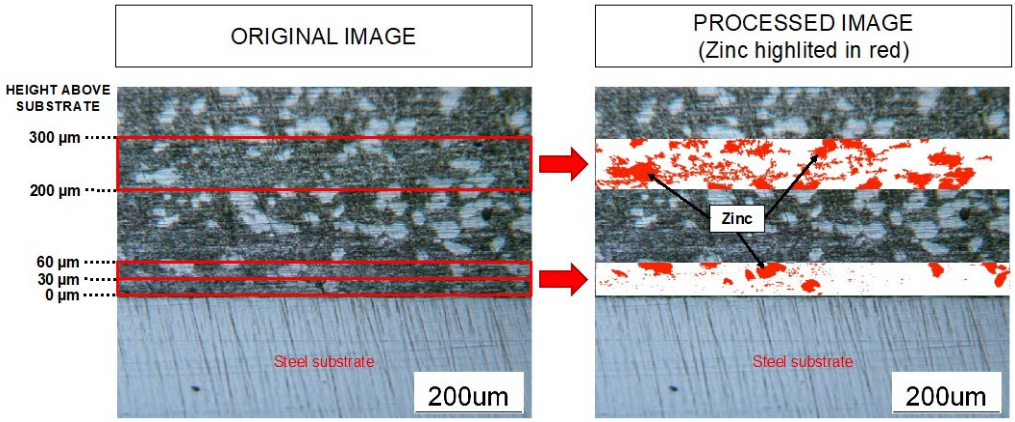

Figure 11. Original image vs ImageJ processed one for Zn40%-Al60% sample. In the two regions of the processed image zinc has been highlighted in red and aluminum in white

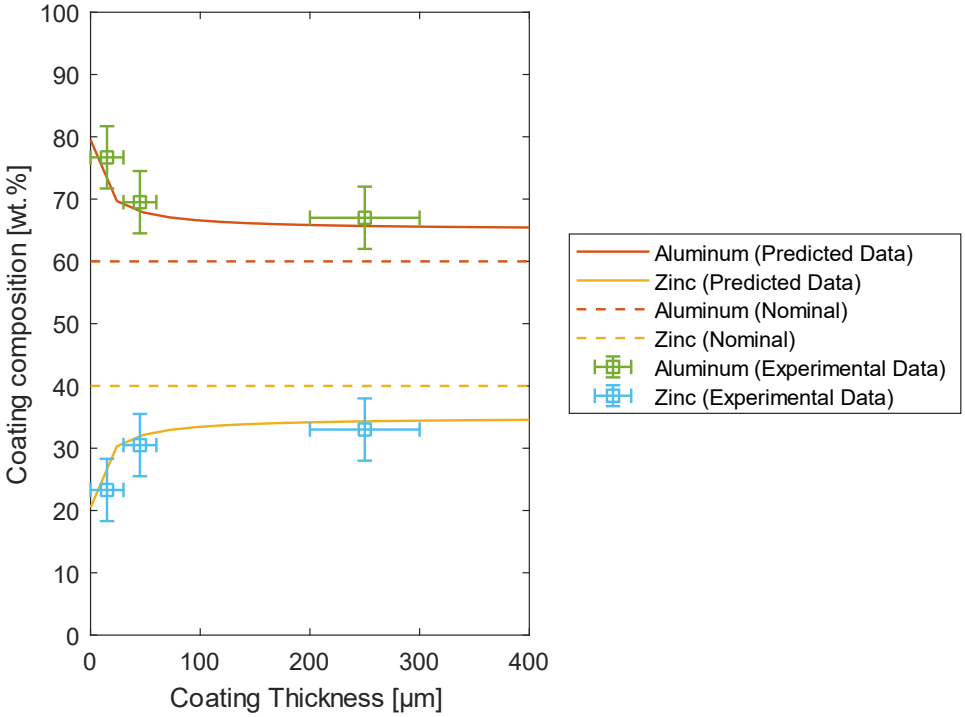

Figure 12. Comparison between the coating composition predicted along the deposit thickness and the experimental data extracted from SEM images for Zn40%-Al60% sample

As predicted by the developed model, the coating composition along the thickness becomes stable only after a certain thickness, approximately around 100 µm. It is observed that during the deposition of the first layers up to a thickness of 40-50 µm, the zinc content is significantly lower with respect to aluminum. This transient layer can become an important aspect in specific applications including corrosion protection coatings, since coating composition in such applications is significant to determine the protective characteristics. In the case of aluminum-zinc coating, a higher aluminum content guarantees longer-lasting and passivation of the coating, while more zinc provides cathodic protection of the substrate [14], [24]. Thus, the lower content of zinc at the first layers, implies that the cathodic protection property of the coating, related to the zinc presence, is stronger for coatings having a thickness higher than 40-50 µm. However, in the case of the deep damages below a thickness of 40-50 µm, the cathodic protection is expected to be lower. To obtain the required coating composition the zinc and aluminum content in the feedstock mixture can be adjusted accordingly based on the prediction of the developed model. Having already calculated the adhesion probabilities for zinc and aluminum particles, it is possible to employ the model to predict the coating composition in correspondence with mixtures with any possible weight fractions of these two constituents.

4. Conclusions

With the aim of estimating the chemical composition of cold spray deposits in the case of mixed feedstock, a hybrid numerical-semi-empirical probability-based approach was developed. The model accounts for the effects of different particle characteristics as well as their corresponding interaction with the substrate. The developed model was experimentally validated in the case of zinc-aluminum mixtures. The results indicated the high accuracy of the model in estimating the deposition efficiency of different zinc-aluminum mixtures. The results also confirmed that the model was also able to predict the evolution of deposit's chemical composition as a function of distance from the substrate.

The model proposed here reinforces the available probabilistic models with finite element impact simulations to account for the morphology and deformation state of individual phases present in the mixture. In addition, it can predict the deposit composition along the entire deposit thickness by considering the process kinetics also during the initial transient phase of interaction with the substrate. This can be of notable significance when the variation of composition through thickness can affect the

deposit performance. For instance, in corrosion protection applications the composition of the inner layers is of vital importance to predict the coating behavior in the eventuality of deep scratches that can expose the underneath substrate. On the other hand, the model can be helpful also for realizing deposits of desired gradient composition.
Future studies will include further experiments on different material mixtures and simulating the real morphology powder particles to better evaluate the model's robustness.

Acknowledgements
AAL and LV contributed equally to this work.

References
[1] W. Li, H. Assadi, F. Gaertner, and S. Yin, "A Review of Advanced Composite and Nanostructured Coatings by Solid-State Cold Spraying Process," *Critical Reviews in Solid State and Materials Sciences*, vol. 44, no. 2. Taylor and Francis Inc., pp. 109–156, Mar. 04, 2019, doi: 10.1080/10408436.2017.1410778.
[2] S. Bagherifard *et al.*, "Design and analysis of additive manufacturedbimodal structures obtained by cold spray deposition," *Addit. Manuf.*, vol. 33, p. 101131, 2020, doi: 10.1016/j.addma.2020.101131.
[3] X. Chu *et al.*, "Understanding the cold spray deposition efficiencies of 316L/Fe mixed powders by performing splat tests onto as-polished coatings," *Surf. Coatings Technol.*, vol. 324, pp. 353–360, 2017, doi: 10.1016/j.surfcoat.2017.05.083.
[4] X. Chu, H. Che, C. Teng, P. Vo, and S. Yue, "A multiple particle arrangement model to understand cold spray characteristics of bimodal size 316L/Fe powder mixtures," *Surf. Coatings Technol.*, vol. 381, 2020, doi: 10.1016/j.surfcoat.2019.125137.
[5] E. Lapushkina and A. Sova, "Effect of powder mixture composition on the deposition efficiency in cold spay: Modelling and experimental validation," *Coatings*, vol. 9, no. 12, 2019, doi: 10.3390/coatings9120832.
[6] A. Sova, R. Maestracci, M. Jeandin, P. Bertrand, and I. Smurov, "Kinetics of composite coating formation process in cold spray: Modelling and experimental validation," *Surf. Coatings Technol.*, vol. 318, pp. 309–314, 2017, doi: 10.1016/j.surfcoat.2016.06.084.
[7] R. Nikbakht, H. Assadi, K. Jahani, M. Saadati, and B. Jodoin, "Cold spray deformation and deposition of blended feedstock powders not necessarily obey the rule of mixture," *Surf. Coatings Technol.*, vol. 424, 2021, doi: 10.1016/j.surfcoat.2021.127644.
[8] S. V. Klinkov, V. F. Kosarev, A. A. Sova, and I. Smurov, "Deposition of multicomponent coatings by Cold Spray," *Surf. Coatings Technol.*, vol. 202, no. 24, pp. 5858–5862, 2008, doi: 10.1016/j.surfcoat.2008.06.171.
[9] H. Koivuluoto and P. Vuoristo, "Effect of powder type and composition on structure and mechanical properties of Cu + Al 2O 3 coatings prepared by using low-pressure cold spray process," *J. Therm. Spray Technol.*, vol. 19, no. 5, pp. 1081–1092, Sep. 2010, doi: 10.1007/S11666-010-9491-2.
[10] J. Wu, H. Fang, S. Yoon, H. Kim, and C. Lee, "The rebound phenomenon in kinetic spraying deposition," *Scr. Mater.*, vol. 54, no. 4 SPEC. ISS., pp. 665–669, 2006, doi: 10.1016/j.scriptamat.2005.10.028.
[11] Y. Xiong, G. Bae, X. Xiong, and C. Lee, "The effects of successive impacts and cold welds on the deposition onset of cold spray coatings," *J. Therm. Spray Technol.*, vol. 19, no. 3, pp. 575–585, Mar. 2010, doi: 10.1007/S11666-009-9455-6.
[12] A. A. Tiamiyu and C. A. Schuh, "Particle flattening during cold spray: Mechanistic regimes revealed by single particle impact tests," *Surf. Coatings Technol.*, vol. 403, p. 126386, Dec. 2020, doi: 10.1016/J.SURFCOAT.2020.126386.
[13] X. Lu, S. Wang, T. Xiong, D. Wen, G. Wang, and H. Du, "Anticorrosion properties of Zn-Al composite coating prepared by cold spraying," *Coatings*, vol. 9, no. 3, p. 210, Mar. 2019, doi: 10.3390/COATINGS9030210.
[14] G. Huang, X. Lou, H. Wang, X. Li, and L. Xing, "Investigation on the cathodic protection effect of low pressure cold sprayed AlZn coating in seawater via numerical simulation," *Coatings*, vol. 7, no. 7, p. 93, Jul. 2017, doi: 10.3390/coatings7070093.

[15] D. Lv, T. Zhang, F. Gong, and A. Olofinjana, "Study on Properties of Cold-Sprayed Al-Zn Coating on S135 Drill Pipe Steel," *Adv. Mater. Sci. Eng.*, vol. 2020, pp. 1–10, Feb. 2020, doi: 10.1155/2020/9209465.
[16] V. Champagne Jr, N. Matthews, and V. Champagne III, "Introduction to supersonic particle deposition," in *Aircraft Sustainment and Repair*, Elsevier, 2018, pp. 799–844.
[17] M. Murugesan and D. W. Jung, "Johnson cook material and failure model parameters estimation of AISI-1045 medium carbon steel for metal forming applications," *Materials (Basel).*, vol. 12, no. 4, p. 609, Feb. 2019, doi: 10.3390/ma12040609.
[18] A. Abbasi-Bani, A. Zarei-Hanzaki, M. H. Pishbin, and N. Haghdadi, "A comparative study on the capability of Johnson--Cook and Arrhenius-type constitutive equations to describe the flow behavior of Mg--6Al--1Zn alloy," *Mech. Mater.*, vol. 71, pp. 52–61, 2014.
[19] J. Xie, D. Nélias, H. W. Le Berre, K. Ogawa, and Y. Ichikawa, "Simulation of the cold spray particle deposition process," *J. Tribol.*, vol. 137, no. 4, Oct. 2015, doi: 10.1115/1.4030257.
[20] A. D. Resnyansky, "An equation of state consistent with the Hugoniot abnormality," in *AIP Conference Proceedings*, 2017, vol. 1793, no. 1, p. 50003.
[21] J. H. Liu, C. X. Huang, S. D. Wu, and Z. F. Zhang, "Tensile deformation and fracture behaviors of high purity polycrystalline zinc," *Mater. Sci. Eng. A*, vol. 490, no. 1–2, pp. 117–125, 2008.
[22] A. Sharma, R. Mishra, S. Jain, S. S. Padhee, and P. K. Agnihotri, "Deformation behavior of single and multi-layered materials under impact loading," *Thin-Walled Struct.*, vol. 126, pp. 193–204, 2018.
[23] H. Assadi *et al.*, "On parameter selection in cold spraying," *Journal of Thermal Spray Technology*, vol. 20, no. 6. pp. 1161–1176, Dec. 2011, doi: 10.1007/s11666-011-9662-9.
[24] D. J. Blickwede, "55\% Al-Zn-alloy-coated sheet steel," *Tetsu-to-Hagané*, vol. 66, no. 7, pp. 821–834, 1980.
[25] E. Lapushkina, "Anti-corrosion coatings fabricated by cold spray technique: Optimization of spray condition and relationship between microstructure and performance," Université de Lyon, 2021.

Appendix

Table A1. Cold spay process parameters used in the literature for spraying zinc-aluminum blends of different compositions

Feedstock combination	Temperature [°C]	Pressure [MPa]	Process gas	Stand of distance [mm]	System type	Ref.
Zn30%-Al70%	410	0.60	Nitrogen	20	Low pressure	[14]
Zn60%-Al40%	410	0.60	Nitrogen	20	Low pressure	[14]
Zn40%-Al60%	400	1.80	Nitrogen	20	High pressure	[13]
Zn60%-Al40%	500	0.80	Nitrogen	15-30	Low pressure	[15]
Zn70%-Al30%	500	0.80	Nitrogen	15-30	Low pressure	[15]
Zn100%	290	2.0	Nitrogen	30	High pressure	[25]
Zn100%	290	2.5	Nitrogen	30	High pressure	[25]
Zn100%	290	3.0	Nitrogen	30	High pressure	[25]

Table A2 - Materials physical properties [19]

Material Name	Density [ton / mm^3]	Shear Modulus [MPa]	Specific Heat [mJ / (ton K)]	Thermal Conductivity [mW / (mm K)]	Inelastic Heat Fraction
Aluminum	2.710 E-09	2.700 E+04	8.980 E+08	237.2	0.900
Zinc	7.136 E-09	4.000 E+04	3.884 E+08	116.9	0.900
St-37 steel	7.830 E-09	7.700 E+04	4.770 E+08	42.70	0.900

Table A3 - Materials equation of state parameters [19], [20], [22]

Material Name	c_0 [mm / s]	s (U_p vs U_s)	$\boldsymbol{\Gamma_0}$
Aluminum	5.386 E+06	1.339	1.970

Zinc	4.600 E+06	1.400	1.600
St-37 steel	4.578 E+06	1.330	1.670

Table A4 - Materials Johnson-Cook parameters [19], [21], [22]

Material	A [MPa]	B [MPa]	C	n	m	T_m [K]	T_{ref} [K]	$\dot{\varepsilon}_{ref}$
Aluminum	148.4	345.5	0.001	0.183	0.895	916.0	298.0	1.000
Zinc	43.67	82.46	0.067	0.204	1.68	692.7	298.0	0.010
St-37 steel	263.5	130.1	0.014	0.092	1.000	1800	293.2	1.000

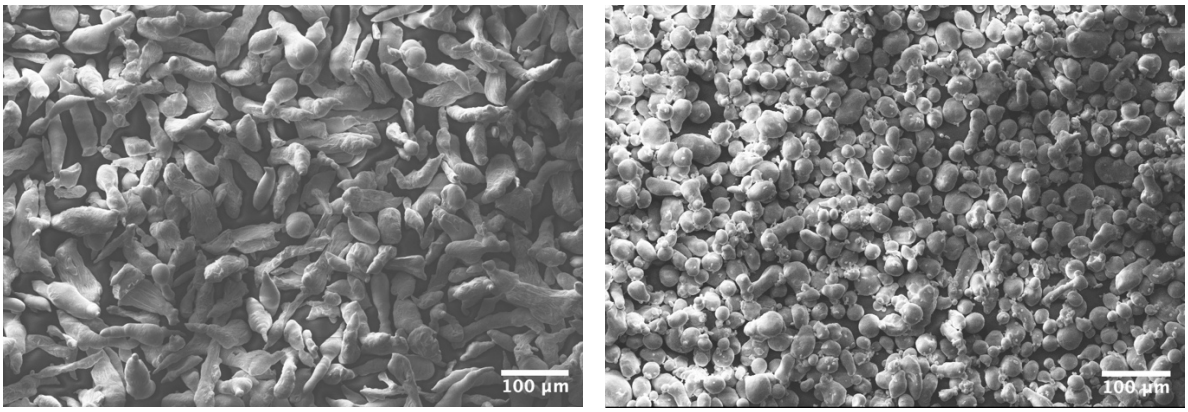

Figure A1. SEM micrographs of Zn (left) and Al (right) powder particles

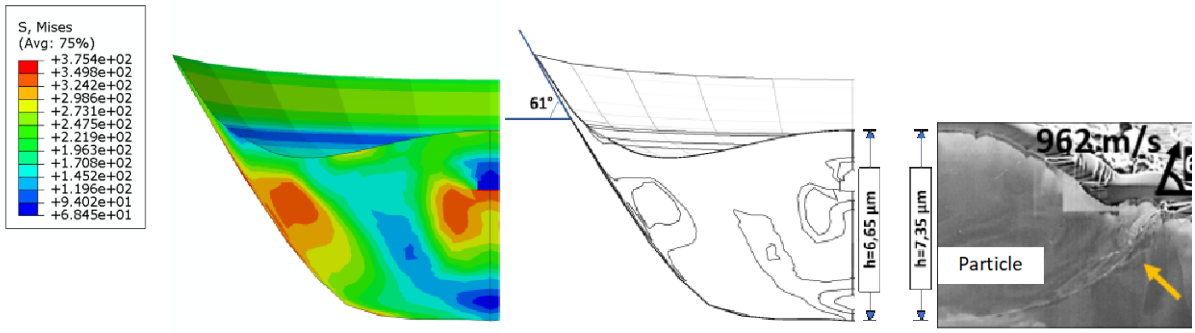

Figure A2. Validation of the numerical model through comparison of the results with the experimental data from [12], FE simulation (Left) and experimental observation (right) of deposited Al particle (D=12.6 µm) on Al substrate with V_p=962 m/s.